



Final Draft **of the original manuscript**

Borba, N.; Kötter, B.; Fiedler, B.; dos Santos, J.F.; Amancio-Filho, S.T.:
Mechanical integrity of friction-riveted joints for aircraft applications.

In: Composite Structures. Vol. 232 (2020) 111542.

First published online by Elsevier: 10.10.2019

<https://dx.doi.org/10.1016/j.compstruct.2019.111542>

Mechanical Integrity of Friction-riveted Joints for Aircraft Applications

N.Z. Borba^a, B. Kötter^b, B. Fiedler^b, J.F. dos Santos^a, S.T. Amancio-Filho^{c,*}

^a Helmholtz-Zentrum Geesthacht – HZG, Centre for Materials and Coastal Research, Institute of Materials Research, Materials Mechanics, Solid State Joining Processes, Geesthacht, Germany

^b Hamburg University of Technology – TUHH, Institute of Polymer and Composites, Hamburg, Germany

^c Graz University of Technology—TU Graz, Institute of Materials Science, Joining and Forming, BMVIT Endowed Professorship for Aviation, Kopernikusgasse 24/1, 8010 Graz, Austria

* Corresponding author: sergio.amancio@tugraz.at; Tel.: +43-316-873-1610; Fax: +43-316-873-7184

Abstract: Composite structures, joined by conventional mechanical fastening techniques, have raised concerns for the aircraft industry. Besides economic and manufacture issues, damage evolution predictability is of great importance. The present work studied friction riveting as an alternative joining technology for composite laminates. The failure and fracture micro-mechanisms of composite laminate single lap joints were studied under quasi-static and cyclic loading. The joints failed mainly by rivet detachment from the composite hole, followed by adhesive/cohesive failure of the squeezed material, and rivet pull-through failure. Despite lower quasi-static strength of friction-riveted joints (6.2 ± 0.3 kN) compared to reference bolted joints (8.7 ± 0.2 kN), their fatigue life was higher by 88%. The main improving contributions were: the squeezed material, working like an adhesive between the composite parts and an additional fracture micro-mechanism, and the absence of clearance at the rivet-composite interface, which promoted an improved load transfer between the joined parts.

Keywords: Friction-riveted joint; Composite laminate; Damage evolution; Quasi-static strength; Fatigue life

1. Introduction

In the past decade, the aircraft design sector embraced the application of carbon-fiber reinforced polymers (CFRPs), owing to the possibility of property tailoring and consequent reduction in structural

weight. In addition, structural components in CFRP provided enhanced strength and stiffness compared to the most traditional designs made of aluminum alloys and flexibility in designing complex shapes [1]. Similar as for aluminum structures, mechanically fastened joints are widely used to assemble composite laminate structures. However, the complex nature of stress fields in the joint vicinities and mechanisms of crack initiation and propagation (*i.e.* delamination, matrix cracking, debonding, fiber breakage) [2] in composite laminates inhibit the failure predictability of such structures and hence the aircraft maintenance programs [3]. Therefore, the failure behavior of bolted joints in composite laminates under different loading conditions has received increased attention. Several empirical [4,5] and numerical studies [6–8] have shown the composite bearing as the desired failure behavior for bolted composite structures due to its comparable higher predictability. By considering this preference, the joint-bearing capability can be enhanced through the optimization of joint geometry (*i.e.*, width, edge-distance, clearance, and washer size) [9,10], composite hole quality [11,12], use of interference-fit bolts [13,14]tightening torque [15], and material layup and properties [1,16]. Moreover, Kelly G. [17] has shown improved bearing strength, stiffness, and fatigue life by combining bolting and bonding joining techniques. The author has addressed the non-catastrophic failure of hybrid joints using low-modules adhesives that allowed load sharing between the bolt and the adhesive along with the retarded fatigue crack initiation, once the bolt carries the more significant load share [17]. Bolted joint properties can also be improved by the through-thickness reinforcement of the composite laminate using z-pins. Li *et al.* [18] have reported the z-pins as an effective method for increasing the joint-bearing properties under quasi-static loading; these pins can also arrest the development of the crack and thereby increase the joint elastic strain energy absorption capacity.

Many works focus on the current concept of entire composite structures with good damage tolerance and fatigue life — both important for the aircraft industry — but there is no consensus on the failure criteria for the empirical analyses of mechanically fastened composite joints. Under quasi-static loading, the bearing strength can be defined as the maximum load during the test following the ASTM D 1602 standard, half of the maximum bearing load, or it can be based on the first peak load, in accordance with the review of Khashaba U.A. [19]. The latter considers undetectable damages in the composite, which propagate in an unstable way after a critical load for the integrity of the plies [20]. In case of cyclic loading, researchers are challenged with the development of the concepts for fatigue life prediction and damage evolution analysis to reduce the effort to develop experimental characterization. Whitworth H.A. [21] has

proposed a concept based on the stiffness degradation of the composite structure. The author has reported that stiffness changes, which can be easily measured, are directly related to damage accumulation and evolution.

Friction riveting is an alternative joining technology suitable for composite laminate structures [22,23]. The process feasibility for several lightweight metallic alloys rivet and polymer composites has been demonstrated [23–27]. Although the quasi-static mechanical properties have been frequently addressed, the fatigue life and damage evolution under both quasi-static and cyclic loading remains as a knowledge gap for friction riveting of composite laminates. Therefore, this work aims to assess the failure behavior under quasi-static and cyclic loading of friction-riveted joints and compare it with the conventional bolted connection. A case study of Ti6Al4V rivets and CF-PEEK overlap parts was investigated. The findings presented here will contribute to further development of prediction models for crack propagation under different loading conditions of friction-riveted joints. These have consequences on the transfer of the technology for large composite structures, and therefore, on its maturity.

2. Materials and methods

2.1. Materials and joining procedure

Single overlap joints were produced using a FricRiveting gantry system (RNA, H. Loitz-Robotik, Germany) coupled with a pneumatic clamping system, where the composite parts were fixed. The overlap configuration comprised 4.34 mm (nominal thickness) carbon-fiber-reinforced polyether-ether-ketone (CF-PEEK) laminates with 58 wt% nominal fiber content in a stacking sequence of $[[(0,90)/(\pm 45)]_3 / (0,90)]_s$ (Toho Tenax Europe GmbH, France). The laminates were joined with extruded plane rivets of Ti6Al4V with a diameter of 5 mm and a length of 60 mm, as schematically shown in Figure 1-a. The M5 stainless steel nut and washer were externally tightened with 1.0-Nm torque to pre-load the joints—this is carried out to minimize through-thickness failure and consequently maximize the joint load capacity [9]. Figure 1-b shows details of the pneumatic clamping device, which consists of two actuators (DZF-50-25-P-A, FESTO, USA), each having a maximum capacity of 1.0 MPa, assembled in a table with the upper element built out of low carbon steel. The clamping system was used to ensure intimate contact between the joining parts during the joining process.

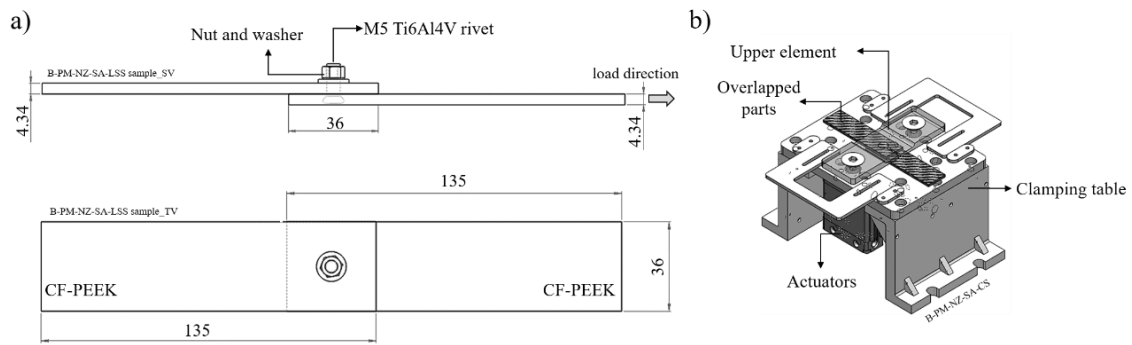


Figure 1. Schematic illustrations of (a) a single lap shear specimen geometry along with the dimensions and load direction (all dimensions are in millimeters) and (b) the pneumatic clamping system used in this work.

Direct friction riveting, a process variant of friction riveting, was used to join the CF-PEEK parts and the Ti6Al4V rivet. The friction riveting process is thoroughly described in previous publications [23,25,28], while the direct friction riveting process was recently published in [22] and applied for an overlap joint configuration. In brief, direct friction riveting consists of frictional heat generated toward the rotating rivet insertion into overlapping composite plates, leading to the plasticization of the rivet tip and its plastic deformation under an increased axial force. Moreover, the molten polymer squeezed between the composite parts and flowing toward the rivet surface during the joining generates adhesion forces at these interfaces after consolidation. The latter together with the rivet anchoring into the composite parts are the main bonding mechanisms of overlap friction-riveted joints. Figure 2 schematically depicts the joining stages.

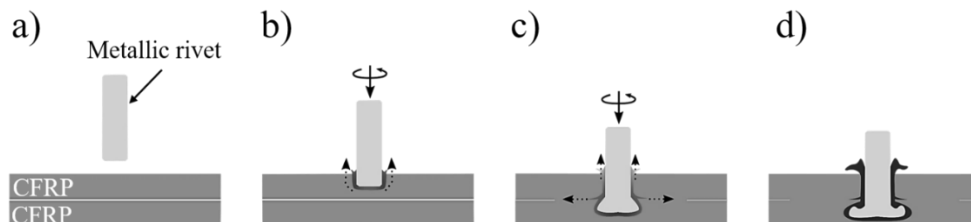


Figure 2. Direct friction riveting steps at different joining stages. a) positioning of the joining parts; b) rivet rotation and insertion through the upper composite (CFRP) part; c) rivet insertion through the lower CFRP part and rivet tip plastic deformation; d) joint consolidation (Adapted from [22]).

The selected joining condition (Table 1) was determined based on the process optimization through the full-factorial design of experiments (2^k with center point) along with analysis of variance. Although the details of such process optimization is beyond the scope of this work and will be published elsewhere, the range of processes parameters used to understand their individual influence on the joint mechanical strength and therefore to optimize the process were: rotational speed – 10,000 to 15,000 rpm, friction force – 5 to 15 kN, clamping pressure – 0.2 to 0.6 MPa, while displacement at friction at steps I and II, as well as consolidation time were kept constant, as shown in Table 1.

Table 1. Selected joining parameters.

Rotational Speed [rpm]	Friction Force I [kN]	Friction Force II, [kN]	Displacement at Friction at Step I [mm]	Displacement at Friction at Step II [mm]	Consolidation Time [s]	Clamping Pressure [MPa]
15,000	5	10	4	3.5	10	0.2

2.2. Global mechanical properties

2.2.1. Single-lap shear testing

Lap shear testing was used to evaluate the quasi-static mechanical performance of the single-lap joints (specimens from Figure 1) according to the ASTM D5961 standard. The test was carried out using a universal testing machine (Zwick 1478, Zwick Roell, Germany) at room temperature (21°C) and a traverse speed of 2 mm/min. The average ultimate lap shear force (ULSF) of three replicates was calculated. The peak force bore by a joint before final failure was considered the ULSF. For the testing, a free distance between the grips of 84 mm was kept constant.

To determine the damage initiation and propagation in the joint upon quasi-static loading, consecutive loading and unloading approach was used. Each specimen was six times loaded at levels of 1.5 kN, 3.0 kN, 4.5 kN, 5.5 kN, 6.5 kN, and 6.8 kN. Three specimens were tested at each load level, with one sample cross-section being analyzed by microscopy. After each level, all the joints were qualitatively inspected by non-destructive testing (NDT) via ultrasound (US) method.

Digital image correlation (DIC) was performed to analyze the out-of-plane strain of friction-riveted joints (ARAMIS 4M, GOM, Germany). The required stochastic speckle pattern on the side surface of the joints (*i.e.* surface through the thickness) was prepared using black ink spray deposited on a white background. A 50-mm focal length lens and a frame rate of 1 Hz were used.

2.2.2. Fatigue experiments

The fatigue tests were carried out using a servo-hydraulic machine (Instron/Schenk, Germany) having ± 10 kN load capacity in a tension-tension regime at $R = 0.1$. A constant amplitude sinusoidal loading at a frequency of 5 Hz was set. Load levels of 60%, 65%, 70%, and 80% of mean ULSF were used to determine the Wöhler curve; below 60%, the endurance limit was achieved for friction-riveted joints. A minimum of three specimens for each level was tested. The single overlap joint configuration, described in Figure 1, was used. The complete joint failure and joint withstanding 10^6 cycles were used as the criteria to stop the test. The joints that survived 10^6 cycles without failure (*i.e.*, run-out specimens) were subsequently tested under quasi-static conditions, as described in Section 2.2.1, and the residual strength reported.

The joint strength was expressed as a ratio between the load level in N and the average of the hole's real area (A_r) for friction-riveted joints, as depicted in Figure 3. The real area of the hole was measured from X-ray tomography images before mechanical testing by using ImageJ software. This approach has already been used by Blaga *et al.* in [23].

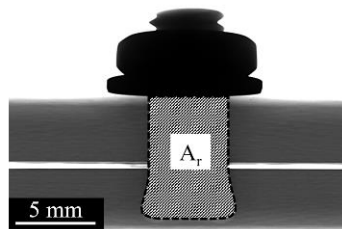


Figure 3. A cross-sectional view of the single-lap joint obtained by X-ray tomography used to measure the real bearing area (A_r).

The variation of joint stiffness was used as an indication of damage accumulation throughout the joint fatigue life. The stiffness degradation calculation of $D = 1 - (E/E_0)$, with E_0 as the initial joint stiffness, was applied.

2.2.3. Statistical analysis of the fatigue life data

The Weibull distribution was used to model the fatigue life of the friction-riveted joints according to the DIN 50100:2016-12 standard. The two-parameter Weibull modeling approach, which considers a set of samples rather than individual results, was applied to the model and confidence estimation. This distribution has been reported in the literature as a useful tool to evaluate the broad scattered fatigue data of composite structures and their reliability [29–31].

The probability density function (PDF) of the two-parameter Weibull distribution is presented in Equation 1. The integration of the PDF results in a cumulative density function (CDF) (Equation 2), which is the probability of joint failure. Equation 3, the reliability function, is derived from Equation 2, with the latter corresponding to the probability of the survival or reliability of a set of joints [29].

$$f(x) = \frac{\beta}{\alpha} \left(\frac{x}{\alpha}\right)^{\beta-1} e^{-\left(\frac{x}{\alpha}\right)^\beta}, \alpha \geq 0, \beta \geq 0 \quad (1)$$

$$F_f(x) = 1 - e^{-\left(\frac{x}{\alpha}\right)^\beta} \quad (2)$$

$$F_s(x) = R_x = 1 - F_f(x) \quad (3)$$

where x is the fatigue life; β is the Weibull slope; α is the characteristic life or the number of cycles in which 63.2% of the sampling is expected to fail; $F_f(x)$ is the probability of failure; and $F_s(x)$ is the probability of survival or reliability (R_x).

Based on the above-mentioned equations, the Weibull distribution and reliability analysis were carried out. In this study, the S-N plots were drawn for R_{99} , R_{90} , and R_{50} .

2.3. Damage and fracture surface analysis

The defects introduced in the joints due to the quasi-static and cyclic loads, such as voids, composite delamination, and broken fibers, were primarily assessed via ultrasound (US) inspection. This measurement was carried out using a C-scan system (USPC 3040 DAC, Dr. Hillger Ingenieurbüro, Germany) with a resolution of 20 MHz and an amplification of up to 106 dB in 0.1 dB steps. Figure 4-a and -b schematically show the set up for the US measurement. The bottom surface of the lower composite plate was scanned, while the upper composite plate was defined as a backing element — *i.e.* ultrasound signals from this region were discarded. Figure 4-c shows a typical cross-sectional view of the as-joined friction-riveted joints along with the defect's depth measurement. The position of the rivet shaft diameter into the lower composite plate was highlighted by a dashed-line circle.

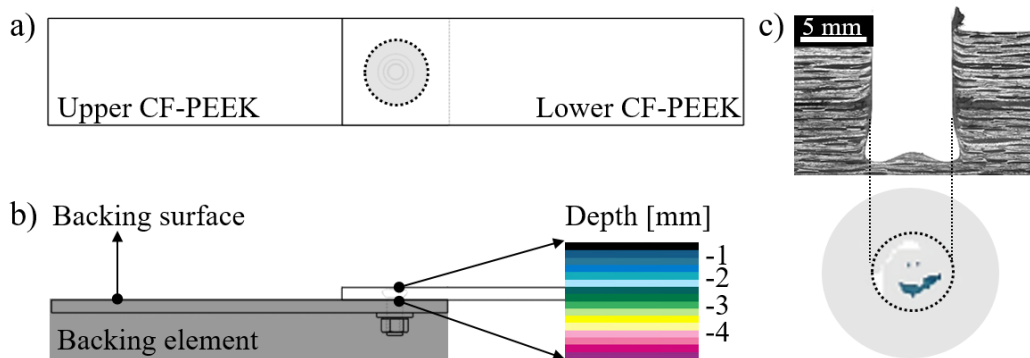


Figure 4. a) Schematic illustration of the joint bottom view highlighting the region of the US measurement. b) Side view of friction-riveted joint showing the selected backing element and the scale of the defect depth based on the lower composite thickness. c) Typical cross-sectional view of the as-joined friction-riveted joint along with the US measurement.

The mid-cross-section of the joints was analyzed by light optical microscopy (LOM) (DM IR microscope, Leica, Germany) to reveal the joint microstructure along with the geometric aspects of the plastic-deformed rivet tip. Scanning electron microscopy (SEM) (Quanta TM FEG 650 equipment) was used to reveal the detailed joint microstructural features and the fracture surface. The samples were prepared following standard materialographic procedures. The joints were sectioned through the center of the rivet, embedded in cold resin, ground and polished to obtain a flat surface finishing. For SEM analysis, the conductivity of the sample surfaces was increased via gold sputtering using a Q150R ES equipment (Quorum Technologies Ltd., England) for 15 s with a current of 65 mA.

A non-destructive evaluation of the friction-riveted joints via X-ray micro-computed tomography (X-ray μ -CT) (Y. Cougar- FeinFocus X-ray system, YXLON, Germany) was carried out to assess the reconstructed three-dimensional models of the failed joints. An operating voltage of 60 kV, a current of 95 μ A, and no filters were hereby applied.

3. Results and discussion

3.1. Mechanical performance under quasi-static loading

The typical force-displacement curve of a single-lap friction-riveted joint is shown in Figure 5-a. The average ultimate lap shear force (ULSF) was 6.2 ± 0.3 kN, which is inferior to the 8.7 ± 0.2 kN of the reference lock-bolted joints, as reported by Borba *et al.* [22]. According to the authors, the combination of through-thickness effect of the bolt shaft along with double-side compression imposed by the large lock-bolt head and collar increases the load bearing capacity of lock-bolted joints in comparison to friction-riveted joints where the plastic deformation at the rivet tip is limited as well as its penetration depth. Three stages characterize the curve: a typical linear elastic behavior until the first load drop (Stage I), followed by an almost linear slope until the peak force is reached (Stage II), and a softening load drop region (Stage III). To analyze the reversibility of the joint strain, which indicates the introduction of damage and plastic deformation during the mechanical test, consecutive load – unload cycles were imposed on the joint. The cross-sectional view of the joints after each cycle (see Figure 5-b) was evaluated to define the main failure mechanisms governing the joint mechanical behavior.

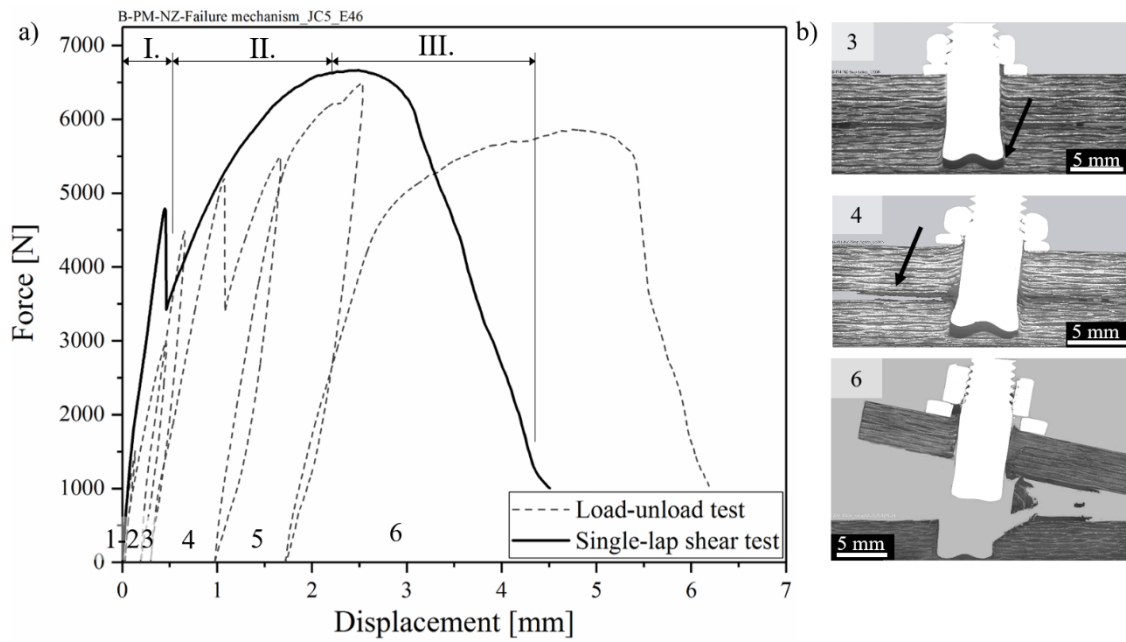


Figure 5. a) Typical lap shear force-displacement curve (solid line) along with six curves from the loading and unloading cycles (dashed line). b) Cross-sectional view of the samples loaded at levels of 4.5 kN, 5.5 kN, and 6.5 kN, which corresponds to cycles 3, 4 and 5.

The loading-unloading curves resulting from the joints loaded up to 4.5 kN (cycle 3 in Figure 5-a) displays a linear elastic behavior with limited unrecovered displacement and no significant change on the elastic modulus. Upon examining the specimen's cross-section of the third cycle (cycle 3 in Figure 5-b), a crack nucleated and propagated throughout the interface between the rivet tip and the composite hole, leading to detachment of the rivet. At the load level of 5.5 kN (cycle 4 in Figure 5-b), which corresponds to the first load drop in the typical load-displacement curve (Stage I in Figure 5-a), the joint stiffness reduces significantly and a considerable plastic deformation is displayed. Such unrecovered deformation combines the adhesive/cohesive failure of the composites interface and the bearing damage introduced through the composite thickness due to the bending moment to which the rivet is subjected (cycle 4 in Figure 5-b). The damage accumulated until the plastic-deformation capacity of CF-PEEK, when the peak force is reached at load level of 6.5 kN (cycle 5 in Figure 5-a). Although the composite was already damaged at this level, the joint still did not fail entirely and was further loaded up to 6.8 kN (cycle 6 in Figure 5-a). Toward the end of this cycle, the composite hole elongated concomitantly with the breakage of the damaged composite and final rivet pull-through failure (cycle 6 in Figure 5-b).

Similar mechanical behavior has been extensively reported in the literature [4,6,32] for hybrid joints and conventional lock-bolted joints of thermoset composites. Although displaying a similar type of behavior, Heimbs *et al.* [4] have shown that for similar single-lap joint geometry using Ti6Al4V bolts with a bolt diameter of 4.8 mm and 130° countersunk head, the displacement at break of the bolted joints is 6.3 mm, which is considerably higher than that in the friction-riveted joints (approximately 44% higher). The broader bolt head in comparison with the plastically deformed rivet tip can partially explain this difference, since it imposes more compression to the composite surface and therefore more restriction to composite-bearing [15].

3.1.1. Damage evolution and failure criteria

The evolution of the overall failure of friction-riveted joints, described in Section 3.1, is related to two main factors, which induce several fracture micro-mechanisms: out-of-plane and in-plane stresses. As the geometry of single-lap joints is non-symmetric (see Figure 6-a), the eccentric tensile load path induces secondary bending, which, in turn, leads to peeling stress [33]. The out-of-plane displacement of the neutral line from the composite parts at different loading times (t_{0-80}) was recorded by DIC and is shown in Figure 6-b. Figure 6-c depicts a lateral view of the deformation fields in the joint during the test. The initial stage t_0 took place prior to the displacement monitoring, which in turn started at t_{20} . The selected loading times correspond to the end of the three stages depicted in the typical load-displacement curve of friction-riveted joint, described in the previous section (Figure 5).

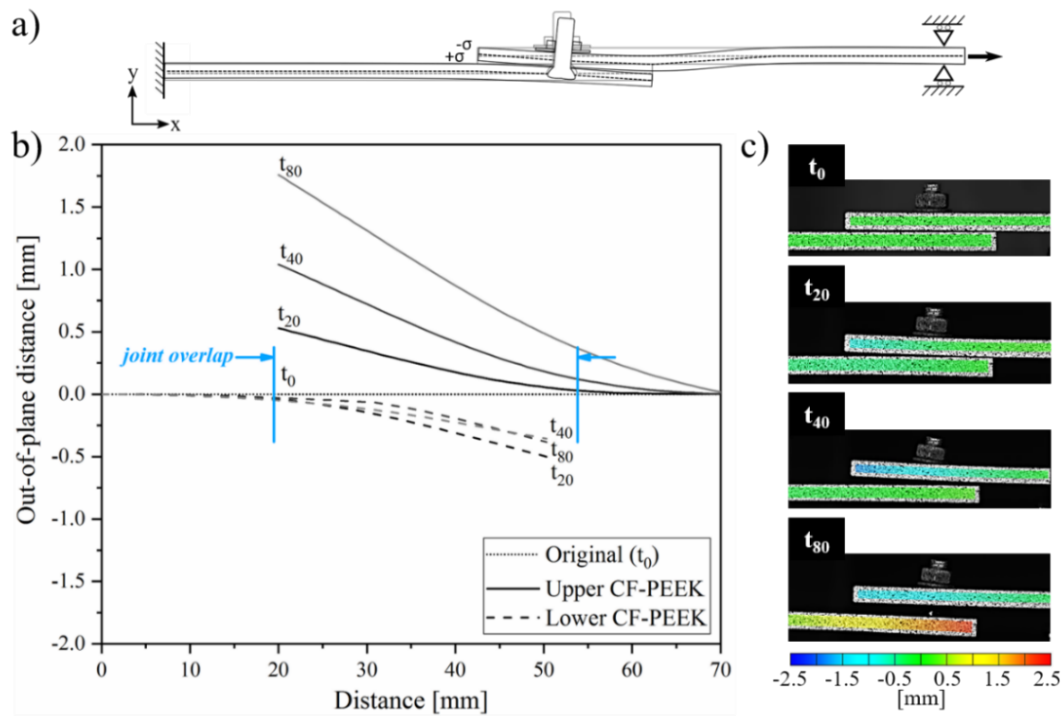


Figure 6. a) Schematic representation of the eccentric loading path in composite overlap friction-riveted joint. b) Out-of-plane displacement curves, and c) respective images of the strain field at different load stages measured by digital image correlation (DIC).

The secondary bending increased with the loading due to a continuous release of the composite surface compression imposed by the pre-tightening torque (*i.e.*, the clamp-up torque), which no longer inhibits the increment of the load eccentricity, thus leading to decrease of joint stiffness. Herrington and Sabbaghian [34] have reported this effect of tightening torque on the mechanical behavior of conventional composite bolted joints. The authors have addressed that the increase in bearing strength coming from an increased clamp-up torque is owing to the out-of-plane constraint that prevent peeling failure [34]. Additionally, the composite parts deflected asymmetrically until the complete rivet removal. At t_{20} (Figure 6-c), such effects led to the brittle fracture of the metal–composite interface through a peel-up of the plies in the composite hole shaft and the rivet detachment, as shown by the fracture surface of the remaining hole in Figure 7-a and -b. The initial separation the composite parts at t_{40} (Figure 6-c) showed to be mainly triggered by peeling stresses which evolved to a large gap between the parts at t_{80} . In the latter step, the rivet is removed from the composite hole, increasing the out-of-plane displacement and imposing bending to the lower composite part.

The fracture analysis of the squeezed material between the composite parts (indicated by the arrow in Figure 7-a) illustrates three main features: a smooth adhesively failed surface (Figure 7-c), an elongated fibrous-like feature not oriented to the loading direction, and exposed fiber bundles in 90° (Figure 7-d). Such features indicate a combination of adhesive and cohesive failure at the composite overlap area. Inside the cohesive failure area, a highly dense ductile fracture of the PEEK matrix by tearing was shown to be one of the primary fracture micro-mechanisms at the composite interface. Additionally, the exposure of the fibers from the composite plate suggests interlaminar cracks inside the first ply of the CF-PEEK owing to cohesive failure. No indication of shear-induced deformation in the squeezed material was identified in this region.

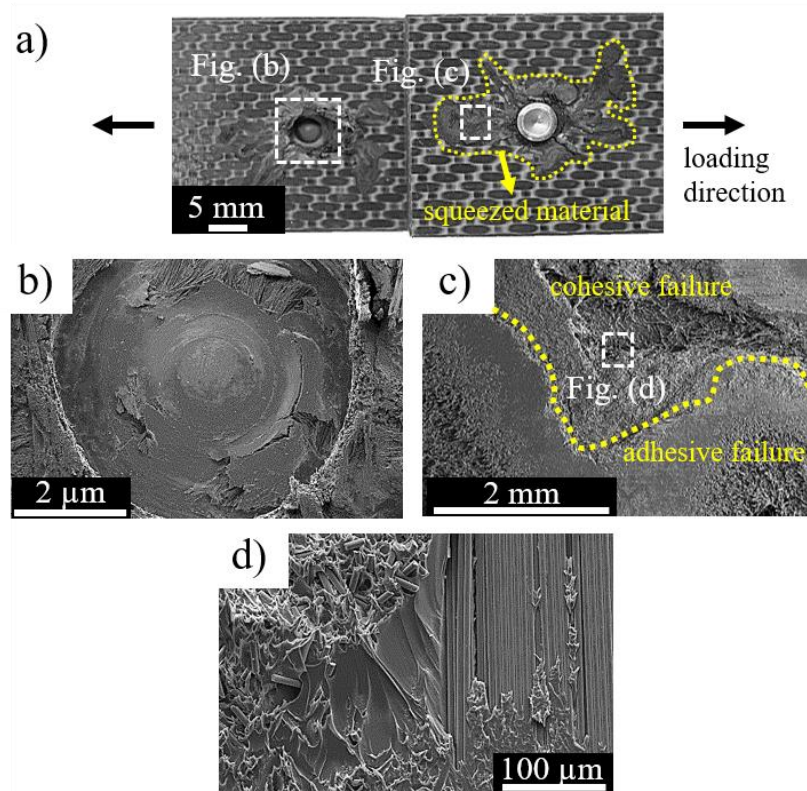


Figure 7. a) Overview of the fracture surface, showing the squeezed material consolidated at the interface between the composite parts. SEM micrographs of the b) hole in the lower composite plate remained from the joining process, c) squeezed material fracture surface, showing the adhesive and cohesive failure regions, and d) PEEK ductile fracture details along with exposed fiber bundles.

By increasing the eccentricity of the load path (from Stage II to Stage III in Figure 5), the in-plane stress became more relevant for joint integrity. Owing to the bending moment, the rotation of the rivet and

the sinking of the plastically deformed rivet tip into the hole shaft walls imposed compression to the composite and through-thickness failure. Figure 8 shows the C-scan measurements of the defect depth in the lower composite part for each stage of the load-displacement curve (Figure 5-a). The dashed-lines highlight the position of the rivet while the white regions in the diagrams correspond to the metal, for which the ultrasound signal is not detectable in the current experiment. In comparison with the as-joined parts (see Figure 4), the out-of-plane stress developed in Stage I did not impose any shear-driven compressive failure on the composite. Therefore, the damaged area remained constant around the rivet. As soon as the rivet rotates in Stage II, the damage was accumulated in the rivet tip vicinities and extended to other plies through the composite thickness (Stage III, Figure 8).

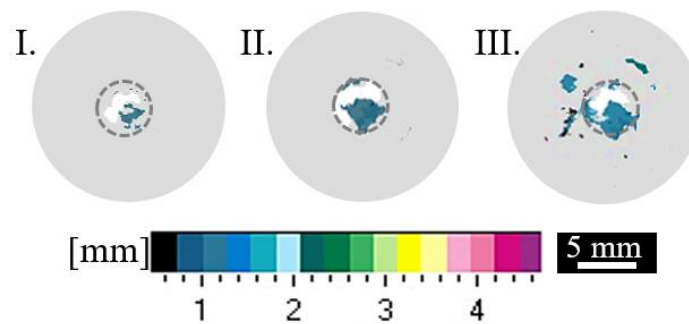


Figure 8. The defect depth acquired via ultrasound inspection in the lower composite part of the overlap friction-riveted joints loaded at levels of 4500 (I), 5500 (II), and 6500 N (III). The images highlighted in dashed-line circles the position of the rivet.

Figure 9 shows the in-plane damages introduced to the joint and their micromechanisms. Critical bearing stress around the composite hole induced high local plastic deformation (*i.e.*, bearing damage), as shown in Figure 9-b. Moreover, the non-uniform bearing stresses across the laminate's thickness (see schematic in Figure 9-c) led to the shear-driven interfacial debonding of the matrix from the fiber bundle oriented in 0° (Figure 9-d) and the kink-band formation (Figure 9-e). CFRP laminates are known to have poor interlaminar strength [1], and the alignment of the fibers to have a significant influence on the composite compression response [7,35]. Although the fibers oriented in 0° can withstand higher compression loads [1], their higher aspect ratio assists the progress of micro-buckling into shear-induced fiber breakage in almost 45° , as observed for the friction-riveted joints. Once this most critical ply in the stack began to fail, the stress was redistributed to the remaining plies, which may fail themselves and

thereby extended such damage — this is clearly seen in Figure 8. Thus, the failure of the laminate occurred progressively until no further loading could be carried, the hole was enlarged, and the rivet was removed from the lower composite part.

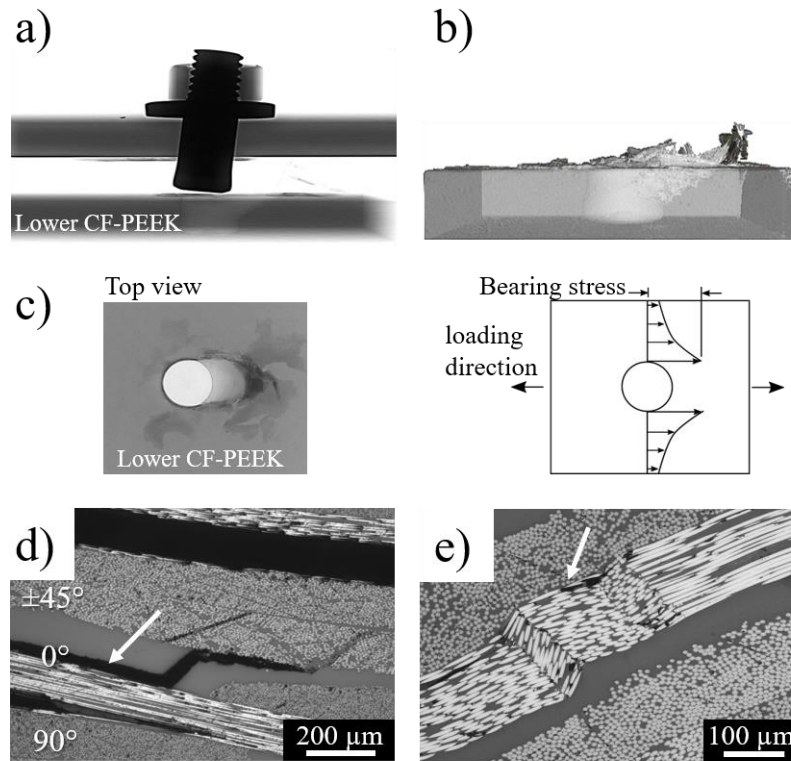


Figure 9. a) Selected X-ray tomography of the friction-riveted joint after the lap-shear test. b) 3D reconstructed μ -CT and c) top view of the lower composite part, highlighting the influence of the bearing stress on the plastically deformed edges of the composite hole. Compression-induced failure of the composite by d) interlaminar damage and e) kink-band formation (indicated by arrow) in fiber bundles orientated in 0° .

The results suggest that the overall failure of the overlap friction-riveted joints under quasi-static shear loading starts with the rivet tip detachment (I, Figure 10-a), followed by the radial crack initiation at the edges of the squeezed material. Such cracks propagate fast through an adhesion region and slow-down in a cohesive failure region (II, Figure 10-a, and Figure 10-b). Furthermore, cohesive failure is transmitted through the composite thickness owing to the compression imposed by the rivet (III, Figure 10-a). Figure 10 illustrates the proposed failure path throughout the bonding zones of the overlap friction-riveted joints.

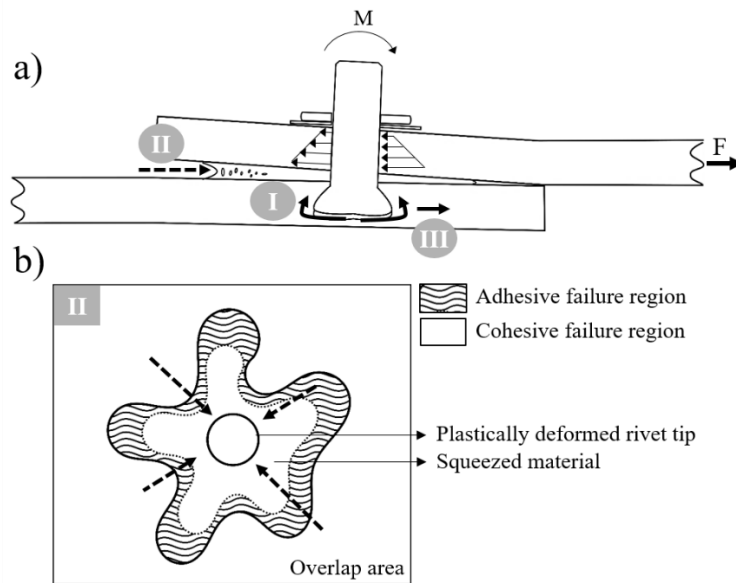


Figure 10. a) Schematic failure path in the overlap friction-riveted joints under shear loading. b) Schematic fracture surface of the overlap area in friction-riveted joints, indicating radial crack propagation from the adhesion to the cohesion failure regions.

One can assume that based on the already described fracture micro-mechanisms, the out-of-plane stress triggered the crack propagation, mainly through the tearing of the PEEK matrix at the initial stages of the quasi-static mechanical test, while the composite's shear-driven compressive failure through the composite thickness dictated the joint integrity, eventually leading to a full rivet pull-out. There is currently no consensus on the critical fracture micro-mechanism, which governs the joint mechanical behavior of composite bolted joints. Consequently the basis to determine their joint failure criteria is also unclear [9]. According to the criteria described by Giannopoulos *et al.* [15], the maximum quasi-static loading to be met in the service of a bolted composite structure, when multiplied by a safety factor of 1.5, has to be less or equal to the specimen's bearing strength. Additionally, in such criteria, this load level is characterized by a quasi-linear and stable region in the typical load-displacement curve [20]. Considering the similarities of friction-riveting and conventional bolted joints regarding the load-displacement curve and failure mode, and thus, assuming similar failure criteria, the allowable failure would be restricted to out-of-plane induced fracture micro-mechanisms at load levels up to 4.5 kN — this is shown by Figure 5-a.

3.2. Mechanical performance under cyclic loading

3.2.1. Fatigue life

The S-N curves acquired for the two-parameter Weibull distribution and different reliability levels (50, 90 and 99%) are shown in Figure 11. In the graph, the arrow indicates the run-out specimens, indicating the fatigue limit. The reliability curves provide the number of cycles that the joint can withstand without failure; they are a useful tool for safe structural design. Statistically, they also represent the life of the weakest member of the population after a specified life in service [36]. For instance, in aircraft structural applications, with very high safety requirements, one can assume that a lower number of cycles is expected at a particular load level along with a conservative design.

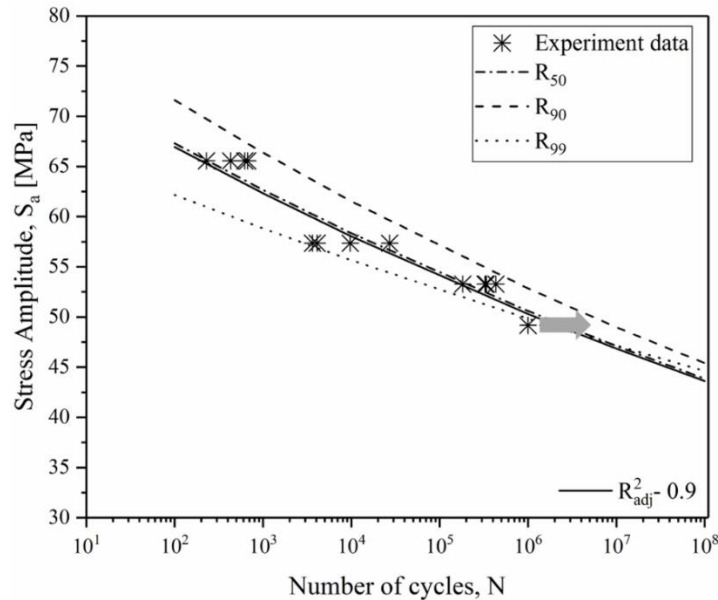


Figure 11. S-N curves acquired for reliabilities of 50%, 90%, and 99% according to the two-parameter Weibull distribution.

The fatigue life at 10^5 cycles is commonly addressed in the aircraft sector to evaluate the performance and certify new designs and joining techniques [37]. For aircraft applications, bolted structures loaded with 30–35% of the quasi-static strength must withstand such fatigue life [37]. The friction-riveted joints reached 10^5 cycles with a stress amplitude of 56 MPa, which corresponds to a load level of 66% of the ultimate quasi-static lap-shear force (ULSF). The result showed an improvement up to

88% for the friction-riveted joints in comparison with the cyclic behavior of conventional mechanical fastening techniques under aircraft requirements. Similar improvement was reported by Mariam *et al.* [38] for dissimilar bolted-bonded hybrid joints of overlapping AA7075 and glass-fiber reinforced epoxy parts. McCarthy *et al.* [39] have reported that the clearance in conventional bolted joints is of maximum concern when designing the limit load of aircraft. According to the authors, joints with a loose-fit hole have a shorter fatigue life than the neat-fit holes once the elongation of the hole is initiated earlier in that scenario. The produced hole (owing to the rivet insertion) of the friction-riveted joints is in intimate contact with the rivet due to the reconsolidation of molten polymeric matrix material at the rivet shaft (Figure 4-c). This feature may provide delayed damage initiation and accumulation in the friction-riveted joints, leading to better cyclic mechanical performance. Additionally, the squeezed material described in Section 3.1.1. (Figure 10) may also act as a failsafe mechanism and provides benefits to structural performance and durability after its failure. This finding is in agreement with the cyclic performance of the bonded-bolted hybrid joints. Chowdhury *et al.* [40] and Kelly G [17] have shown that hybrid bolted-bonded joints have the highest fatigue life in comparison with bolted and bonded joints. In both studies, the presence of the fastener in a hybrid bolted-bonded joint reduced the peel stress and arrested the crack propagation in the bond line, which increased two times the number of cycles to the final failure.

The endurance limit was considered when the joints survived one million cycles without failure. One can assume that after this value, the joint would no longer be damaged by fatigue and thus the test was interrupted. This hypothesis was verified through the quasi-static residual strength of the run-out specimens. The results are presented in Table 2 **Error! Reference source not found.** By comparing the residual strength after one million cycles (5.9 ± 0.3 kN) with the quasi-static strength (ultimate lap shear force, ULSF) (6.2 ± 0.3 kN) of the joints, no statistically significant variation of the mechanical performance was identified. The result indicates that the loading level, which the surviving joints underwent after one million cycles, did not induce any critical fatigue damage in the joint, not compromising its mechanical integrity.

Table 2. Quasi-static residual strength of run-out friction-riveted joints.

Ultimate Lap Shear Force (ULSF)	[kN]
Quasi-static lap-shear testing	6.2 ± 0.3

ULSF after 10^6 cycles	5.9 ± 0.3
--------------------------	---------------

3.2.2. Stiffness degradation and damage evolution

The friction-riveted joints failed similarly under the cyclic test as in the quasi-static test: failure of the squeezed material followed by bearing of the composite and rivet pull-out. The fatigue damage evolution and the fracture micromechanisms associated with the failure mode were assessed using the stiffness degradation approach [21]. Typical degradation curves for the joints loaded at different stress levels are shown in Figure 12. Despite the four-stage curve, the extent of each stage relative to different fracture micromechanisms is dependent on the applied load (Figure 12-a). At a stress level of 80% of the ULSF, the critical damage was early introduced on the joint, shifting the stiffness degradation curve toward lower fatigue cycles, while at lower stress levels the crack initiation and propagation were postponed toward a higher fatigue cycles. Moreover, the number of stages in such stress level is reduced to three — it indicates that the load level is superior to the critical level that triggers the first fracture micro-mechanism. Each stage was described for the joints loaded at the low-stress level of 66% of ULSF, as presented in Figure 12-b. At this load level, all four stages of degradation are visible and stable, and therefore selected for further microstructural analyses.

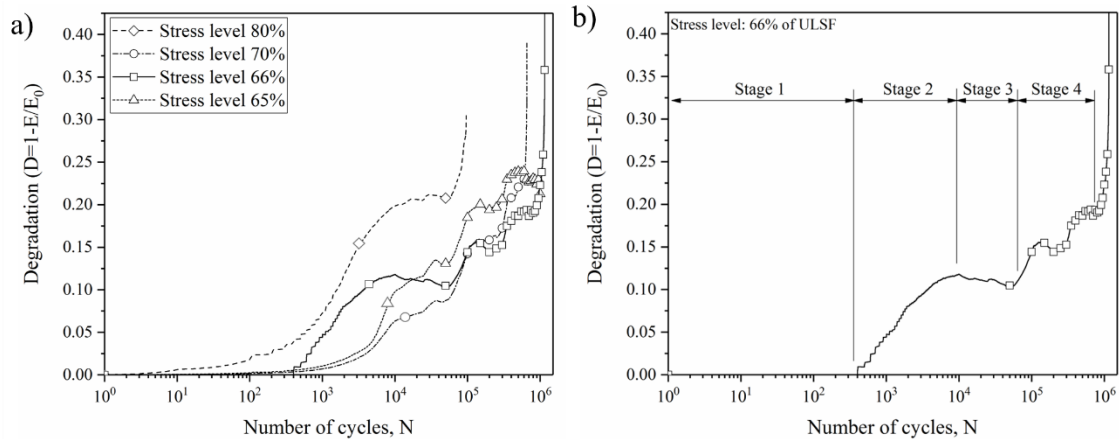


Figure 12. Stiffness degradation curves for a) different stress levels and b) for 66% of the ULSF, showing the stages of damage evolution.

The fracture analyses of friction-riveted joints after each damage stage from Figure 12-b are presented in Figure 13. The joint at the end of Stage 4 failed completely, and therefore, its fracture analysis was herein neglected. In the initial stage, up to 1.5×10^2 cycles (Figure 12-b), the consolidated squeezed material between the composite joining parts failed, followed by an adhesive failure of the rivet from the composite hole (Figure 13-a and -b). After the damage initiation, the second stage displayed an almost linear slope until the plateau was reached (Stage 2, Figure 12-b), at 10^4 cycles. At this stage, the cracks already developed from beneath the rivet and from the squeezed material are believed to propagate toward the interface between the rivet and the composite over different fatigue crack fronts, as indicated by solid-line arrows in Figure 13-d. The cracks are mainly oriented at 45° to the loading direction and located between the reconsolidated composite material and the composite matrix. Such cracks no longer propagated after reaching the rivet shaft, which, in turn, arrested them and stabilized the joint stiffness until 10^5 cycles (Stage 3, Figure 12-b). Finally, owing to the momentum imposed on the rivet, the compression-induced cracks were spread through the composite thickness, thereby leading to intralaminar defects in fiber bundles oriented at 90° to the loading direction (Figure 13-e and -f). This fiber bundle-orientation carried less tension and compression, as it is significant only for transversal loads and structure stability [14].

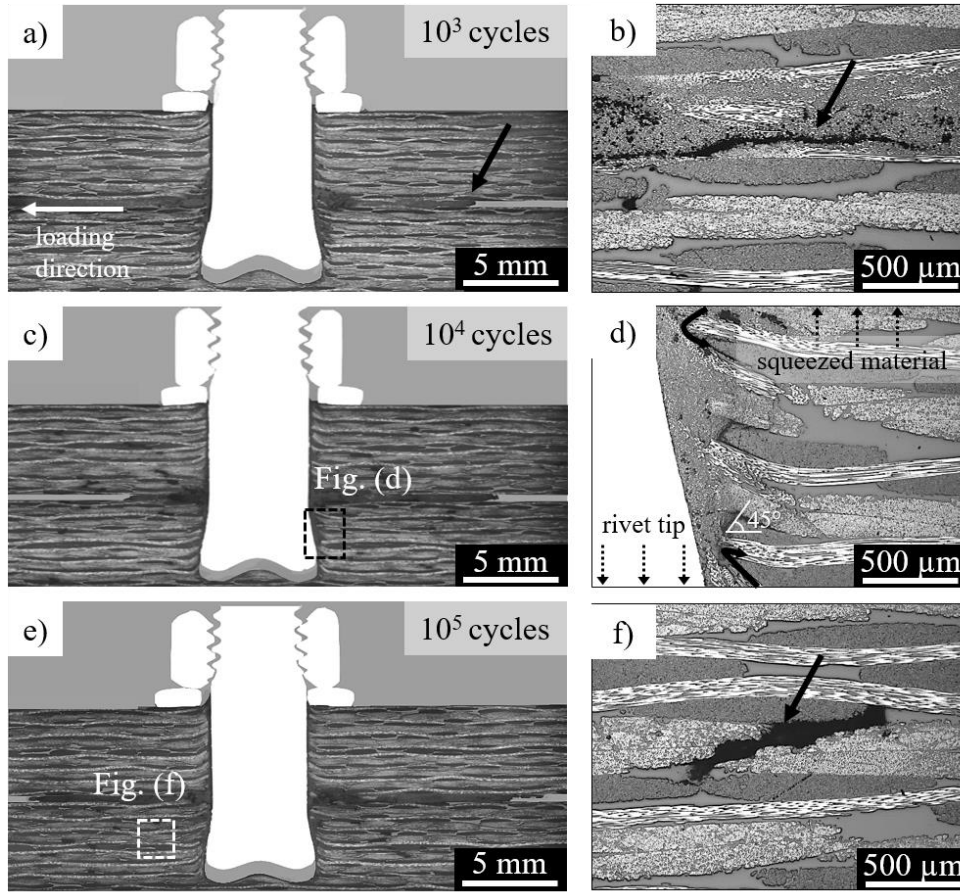


Figure 13. Overview of the joint cross-sections after 10^3 , 10^4 , and 10^5 cycles (a-e) and details of the corresponding fracture mechanisms (b-f), highlighted by solid-line arrows. Additional dashed-line arrows in (d) illustrate the squeezed material and rivet tip locations, which are not depicted in the image. All the joints were loaded with 66% of ULSF.

The micromechanisms involved in the damage evolution and failure of friction-riveted joints were addressed in Figure 14. Despite the propagation of the fatigue crack by a mixture of adhesive-cohesive failure in the squeezed material, contrary to the joint mechanical behavior under quasi-static loading, mainly shear-induced deformation was identified in the cohesive failure region. Figure 14-b shows a periodic wave-like pattern of the matrix along the loading direction, which is well known in the literature as *hackles* [41]. On continued cyclic loading of ductile materials, shear-induced cracks are generally formed in the matrix between fibers. When they coalesce, they form microvoids along with highly plastic-deformed waves, as detailed in Figure 14-c. Simultaneously, cracks nucleated underneath the rivet tip, where the stress concentration is expected to be higher [28], leading to adhesive failure of the rivet-composite hole interface (Figure 14-d). Although the fracture surface of the composite hole showed plastic

deformation of the matrix, no out-of-plane tearing of fibrils was observed (Figure 14-e), indicating less influence of the out-of-plane stress.

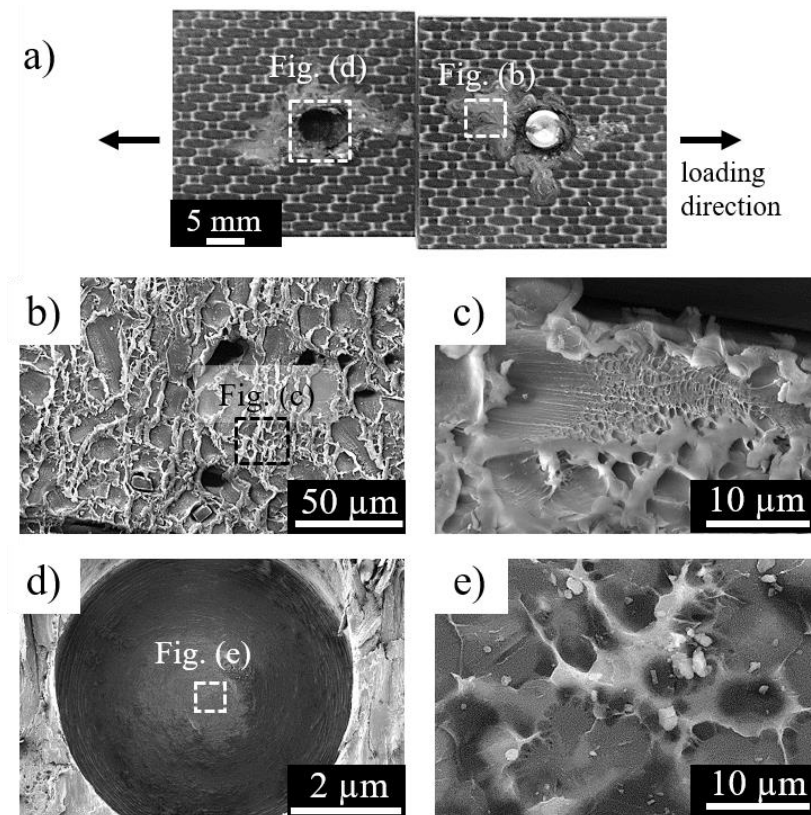


Figure 14. a) Overview of a high cycle fatigue fracture surface (456824 cycles to failure). SEM micrographs of the b) squeezed material fracture surface, which shows the hackle formation and detailed in c), d) hole in the lower composite plate remained from the joining process, and d) details of the plastic deformed matrix in the composite hole.

Kelly G [17] has published similar failure mode and damage evolution for bolted-bonded hybrid joints. Owing to a larger adhesion area between the joining parts resulting from the applied adhesive, the crack initiation was delayed for higher fatigue life in comparison with the friction-riveted joints.

Based on the results, under cyclic loading, the friction-riveted joints failed mainly by shear-induced defects while under quasi-static loading, a combination of in-plane and out-of-plane induced defects was observed. Regarding the failure criteria and consequently the design of the friction-riveted joints for fatigue, fracture mechanics similarly applied to the mechanically fastened composite must be assessed. However, this is beyond the scope of this paper. The description of the complex failure mode and

fracture micromechanisms presented herein can be further used to predict the progressive failure of the joints by using finite element methods; it also assists the strain energy release rate analysis. This topic is an ongoing investigation and will be published elsewhere.

4. Conclusions

The mechanical behavior under quasi-static and cyclic loading of the friction-riveted joints in composite laminates was described in this paper. Two features of such joints were considered relevant to understand the damage evolution in lap-shear quasi-static and fatigue tests: the squeezed material, which worked like an adhesive, along with its failure as an additional fracture micromechanism, and the plastically deformed rivet that arrested the crack propagation, especially under cyclic loading.

The friction-riveted joints presented up to 40% lower ultimate lap shear force (6.2 ± 0.3 kN) and reduced displacement at a break in comparison with the bolted joints. Less efficient superficial compression on the friction-riveted joints in comparison to the clamp-up of the bolt head in conventional bolts along with less penetration of the rivet into the composite in friction-riveted joints may lead to less through-thickness load-carrying capacity and hence inferior joint strength. For quasi-static loading, three main stages defined the mechanical behavior, associated with the rivet debonding, followed by a mixture of adhesive and cohesive failure of the squeezed material, and finally, a pull-through of the rivet.

Despite lower ultimate lap shear forces under of quasi-static loading, the fatigue life of friction-riveted joints improved significantly, by 88% in comparison with the published works on lock-bolted joints. The intimate contact between the rivet and composite hole by the reconsolidated molten polymer may explain the improvement in fatigue life and fatigue strength of the friction-riveted joints. Overall, friction-riveted joints failed in a similar manner under cyclic and quasi-static loading, except for more shear-induced damage in the last scenario. No critical fatigue damage was induced to run-out specimens, thus reflecting similar residual strength (5.9 ± 0.3 kN), as the quasi-static ultimate lap shear force (6.2 ± 0.3 kN). The stiffness degradation curve over fatigue life showed four typical stages where damage is accumulated under different fracture micromechanisms, including shear-induced plastic deformation at the fiber-matrix interface and intralaminar defects distant to the joining area, in fiber bundles oriented at 90° .

Friction riveting presented an improved fatigue life in comparison with conventional bolted joints and thus proved to be an alternative joining technology for composite laminates. This work provides a description of the complex failure modes and fracture mechanisms, which can assist on establishing and validating prediction models for progressive failure of composite friction-riveted joints under quasi-static and cyclic loading.

Acknowledgments

The authors would like to acknowledge the financial support from the National Council for Technological and Scientific Development- CNPq (Brazil) [grant number 200695/2015-0] and the Helmholtz Association through the Young Investigator Group, “Advanced Polymer Metal Hybrid Structures” [grant number VH-NG-626]. Sergio T. Amancio-Filho would like to acknowledge "the Austrian aviation programme TAKE OFF" and "BMVIT-Austrian Ministry for Transport, Innovation, and Technology" for the financial support.

References

- [1] Niu MC-Y. *Airframe Structural Design: Practical Design Information and Data on Aircraft Structures*. Hong Kong Conmilit Press LTD.; 1988.
- [2] Tsotsis TK. 8 - Considerations of failure mechanisms in polymer matrix composites in the design of aerospace structures. *Fail. Mech. Polym. Matrix Compos.*, Woodhead Publishing; 2012, p. 227–78.
- [3] Breuer UP. *Commercial Aircraft Composite Technology*. Springer International Publishing; 2016.
- [4] Heimbs S, Schmeer S, Blaurock J, Steeger S. Static and dynamic failure behaviour of bolted joints in carbon fibre composites. *Compos Part Appl Sci Manuf* 2013;47:91–101.
- [5] Skorupa A, Skorupa M, Machniewicz T, Korbel A. Fatigue crack location and fatigue life for riveted lap joints in aircraft fuselage. *Int J Fatigue* 2014;58:209–17.
- [6] Hu XF, Haris A, Ridha M, Tan VBC, Tay TE. Progressive failure of bolted single-lap joints of woven fibre-reinforced composites. *Compos Struct* 2018;189:443–54.
- [7] Nerilli F, Vairo G. Progressive damage in composite bolted joints via a computational micromechanical approach. *Compos Part B Eng* 2017;111:357–71.
- [8] Yang Y, Liu X, Wang Y-Q, Gao H, Li R, Bao Y. A progressive damage model for predicting damage evolution of laminated composites subjected to three-point bending. *Compos Sci Technol* 2017;151:85–93.
- [9] Khashaba UA, Sallam HEM, Al-Shorbagy AE, Seif MA. Effect of washer size and tightening torque on the performance of bolted joints in composite structures. *Compos Struct* 2006;73:310–7.

- [10] Cooper C, Turvey GJ. Effects of joint geometry and bolt torque on the structural performance of single bolt tension joints in pultruded GRP sheet material. *Compos Struct* 1995;32:217–26.
- [11] Saleem M, Zitoune R, El Sawi I, Bougherara H. Role of the surface quality on the mechanical behavior of CFRP bolted composite joints. *Int J Fatigue* 2015;80:246–56.
- [12] Camanho P, Tong L. *Composite Joints and Connections | Principles, Modelling and Testing*. Woodhead Publishing. 2011.
- [13] Mann JY, Machin AS, Lupson WF, Pell RA. *The Use of Interference-Fit Bolts or Bushes and Hole Cold Expansion for Increasing the Fatigue Life of Thick-Section Aluminium Alloy Bolted Joints*. Aeronautical Research Labs Melbourne (Australia); 1983.
- [14] Raju KP, Bodjona K, Lim G-H, Lessard L. Improving load sharing in hybrid bonded/bolted composite joints using an interference-fit bolt. *Compos Struct* 2016;149:329–38.
- [15] Giannopoulos IK, Doroni-Dawes D, Kourousis KI, Yasae M. Effects of bolt torque tightening on the strength and fatigue life of airframe FRP laminate bolted joints. *Compos Part B Eng* 2017;125:19–26.
- [16] Knoll JB, Riecken BT, Kosmann N, Chandrasekaran S, Schulte K, Fiedler B. The effect of carbon nanoparticles on the fatigue performance of carbon fibre reinforced epoxy. *Compos Part Appl Sci Manuf* 2014;67:233–40.
- [17] Kelly G. Quasi-static strength and fatigue life of hybrid (bonded/bolted) composite single-lap joints. *Compos Struct* 2006;72:119–29.
- [18] Li R, Huong N, Crosky A, Mouritz AP, Kelly D, Chang P. Improving bearing performance of composite bolted joints using z-pins. *Compos Sci Technol* 2009;69:883–9.
- [19] Khashaba UA. In-plane shear properties of cross-ply composite laminates with different off-axis angles. *Compos Struct* 2004;65:167–77. doi:10.1016/j.compstruct.2003.10.012.
- [20] Maksimović S. Some computational and experimental aspects of optimal design process of composite structures. *Compos Struct* 1990;16:237–58.
- [21] Whitworth HA. A stiffness degradation model for composite laminates under fatigue loading. *Compos Struct* 1997;40:95–101.
- [22] Borba NZ, Blaga L, dos Santos JF, Amancio-Filho ST. Direct-Friction Riveting of polymer composite laminates for aircraft applications. *Mater Lett* 2018;215:31–4.
- [23] Blaga L, dos Santos JF, Bancila R, Amancio-Filho ST. Friction Riveting (FricRiveting) as a new joining technique in GFRP lightweight bridge construction. *Constr Build Mater* 2015;80:167–79.
- [24] Altmeyer J, Suhuddin UFH, dos Santos JF, Amancio-Filho ST. Microstructure and mechanical performance of metal-composite hybrid joints produced by FricRiveting. *Compos Part B Eng* 2015:130–40.
- [25] Rodrigues CF, Blaga LA, dos Santos JF, Canto LB, Hage E, Amancio-Filho ST. FricRiveting of aluminum 2024-T351 and polycarbonate: Temperature evolution, microstructure and mechanical performance. *J Mater Process Technol* 2014;214:2029–39.
- [26] Proença B, Blaga L, Canto LB, Dos Santos JF, Amancio-Filho ST. Force controlled Friction Riveting of glass fiber reinforced polyamide 6 and aluminum alloy 6056 hybrid joints, Orlando: 2015.
- [27] Amancio-Filho ST. Friction Riveting: development and analysis of a new joining technique for polymer-metal multi-material structures. *Welding in the World* 2011;55:13–24.

- [28] Amancio-Filho ST. Henry Granjon Prize Competition 2009 Winner Category A: “Joining and Fabrication Technology” Friction Riveting: development and analysis of a new joining technique for polymer-metal multi-material structures. *Weld World* 2011;55:13–24.
- [29] Dirikolu MH, Aktaş A, Birgoren B. Statistical analysis of fracture strength of composite materials using Weibull distribution. *Turk J Eng Environ Sci* 2002;26:45–8.
- [30] Naresh K, Shankar K, Velmurugan R, Gupta NK. Statistical analysis of the tensile strength of GFRP, CFRP and hybrid composites. *Thin-Walled Struct* 2018;126:150–61.
- [31] Jiang H, Luo T, Li G, Zhang X, Cui J. Fatigue life assessment of electromagnetic riveted carbon fiber reinforce plastic/aluminum alloy lap joints using Weibull distribution. *Int J Fatigue* 2017;105:180–9.
- [32] Egan B, McCarthy CT, McCarthy MA, Gray PJ, O’Higgins RM. Static and high-rate loading of single and multi-bolt carbon–epoxy aircraft fuselage joints. *Compos Part Appl Sci Manuf* 2013;53:97–108.
- [33] Skorupa A, Skorupa M. Secondary Bending for Mechanically Fastened Joints with Eccentricities. *Riveted Lap Jt. Aircr. Fuselage*, Springer, Dordrecht; 2012, p. 145–84.
- [34] Herrington PD, Sabbaghian M. Effect of Radial Clearance between Bolt and Washer on the Bearing Strength of Composite Bolted Joints. *J Compos Mater* 1992;26:1826–43.
- [35] Awadhani LV, Bewoor A. Parametric study of composite bolted joint under compressive loading. *Procedia Manuf* 2018;22:186–95.
- [36] Determining the fatigue life of composite aircraft structures using life and Load-enhancement factors - Report 2011.
- [37] Schmidt-Brandecker B, Schmidt H. *Fatigue & Damage Tolerance* 2017.
- [38] Mariam M, Afendi M, Abdul Majid MS, Ridzuan MJM, Gibson AG. Tensile and fatigue properties of single lap joints of aluminium alloy/glass fibre reinforced composites fabricated with different joining methods. *Compos Struct* 2018;200:647–58.
- [39] McCarthy MA, Lawlor VP, Stanley WF. An Experimental Study of Bolt-Hole Clearance Effects in Single-lap, Multibolt Composite Joints, An Experimental Study of Bolt-Hole Clearance Effects in Single-lap, Multibolt Composite Joints. *J Compos Mater* 2005;39:799–825.
- [40] Chowdhury NM, Wang J, Chiu WK, Chang P. Static and fatigue testing bolted, bonded and hybrid step lap joints of thick carbon fibre/epoxy laminates used on aircraft structures. *Compos Struct* 2016;142:96–106.
- [41] Plumtree A, Shi L. Fatigue damage evolution in off-axis unidirectional CFRP. *Int J Fatigue* 2002;24:155–9.